JOURNAL OF Materials CHEMISTRY

Displacement cascades in $Gd_2Ti_2O_7$ and $Gd_2Zr_2O_7$: a molecular dynamics study

John A. Purton*[a] and Neil L. Allan[b]

[a]*CLRC, Daresbury Laboratory, Keckwick Lane, Warrington, UK WA4 4AD. E-mail: j.a.purton@dl.ac.uk*
[b]*School of Chemistry, University of Bristol, Cantock's Close, Bristol, UK BS8 1TS. E-mail: n.l.allan@bris.ac.uk*

Received 29th January 2002, Accepted 26th July 2002
First published as an Advance Article on the web 23rd August 2002

We report molecular dynamics simulations of the production of radiation cascades in two pyrochlore compounds that have been proposed as possible materials for high level radioactive waste storage. There are clear differences between the two systems that support the results of recent high energy ion bombardment experiments, in which pyrochlores were increasingly radiation resistant with increasing Zr content.

Introduction

Disposal of the plutonium generated by the nuclear fuel cycle remains one of the most daunting environmental challenges of this century[1,2] since it is a long-lived environmental contaminant (half-life ^{239}Pu 24 100 years), is fissile (bare critical mass 15 kg of metal) and decays to longer-lived and also fissile ^{235}U (half-life 7×10^8 years). The global inventory of Pu is $\sim$1300 tonnes and the dismantling of nuclear warheads following the Cold War will contribute a further 100 tonnes. Substantial amounts of Pu will require immobilisation in a solid matrix for geological disposal, together with other actinides such as Np and Am. Immobilisation requires the radionuclides be bound in an inert matrix capable of retaining its structural integrity during prolonged heavy particle bombardment at temperatures of $\sim$300–600 K. The identification of a suitable host matrix is a contentious issue. For example, US government-sponsored research has identified the pyrochlore $Gd_2Ti_2O_7$ as a primary candidate. However, several studies[3] employing heavy ion bombardment to simulate the effects of α-decay have demonstrated that this compound undergoes amorphisation at a dose corresponding to that of α-decay damage, resulting in a subsequent tenfold increase in the leach rate of Pu. Wang *et al.*[4] have also used heavy ion bombardment to demonstrate striking variation in radiation tolerance in the series $Gd_2(Zr_xTi_{1-x})_2O_7$ (x = 0–1). Increasing radiation tolerance was found with increasing Zr content, such that $Gd_2Zr_2O_7$ was predicted to withstand radiation damage for 30 million years, compared with 800 years for $Gd_2Ti_2O_7$. A comparison of $Gd_2Ti_2O_7$ and $Gd_2Zr_2O_7$ is the purpose of the present paper. In contrast, Sickafus *et al.*[5] have proposed that fluorite compounds, sharing the basic $A_2B_2O_7$ structure as pyrochlores but with a different cation arrangement, have a greater propensity for resisting radiation damage. The A^{3+} and B^{4+} ions in these fluorites are similar in size and it has been suggested this leads to a more disordered structure which is less perturbed by radiation damage. However, Weber and Ewing[6] have concluded that the energy barrier to damage recovery rather than the fluorite structure itself is critical. The properties of members of the series $Gd_2(Zr_xTi_{1-x})_2O_7$ are thus receiving increasing attention.[7,8]

Two types of particle irradiation[9] cause the α-decay damage. The first is the α-particle or helium ion, with an energy of 4.5 to 5.8 MeV and a range of 10–30 μm. The second is the recoil of the heavy actinide nucleus, which has an energy of 70–100 keV and a range of 10–20 nm. In order to determine the amount of radiation damage, it is important to establish whether each particle will transfer its energy to electrons (*via* electronic excitation and ionisation) or to atomic nuclei by elastic collisions. An α-particle deposits its energy predominantly by ionisation over its path, with a limited number of elastic collisions ($\sim$100) at the end of its trajectory, while an α-recoil ion will lose most of its energy by elastic collisions, producing up to several thousand atomic displacements.

The initial step in the radiation damage process is the production of a 'primary knock-on' atom (PKA). The PKA dissipates its energy through elastic interactions with 'target' atoms and, if the PKA has sufficient kinetic energy (and mass), leads to the formation of an atomic collision cascade.[9] The subsequent damage evolution hinges on two important factors. The first is the degree to which lattice stability is affected by the accumulation of point defects (*i.e.* its propensity to amorphise under irradiation). The second factor concerns the ultimate fate of the irradiation-induced point defects, which can migrate and annihilate harmlessly or can cluster with other interstitials and vacancies to precipitate dislocation loops and voids. The final damaged state is the result of the initial cascade (femtoseconds), nearly instantaneous relaxation of the structure (picoseconds) and the thermal annealing (seconds).

Atomistic simulations have been demonstrated to provide valuable insight into the behaviour of materials on the atomic scale and are especially useful where experiment is limited by high pressures, temperatures or toxicity. Molecular dynamics (MD) has been used to study the formation of defect cascades in metals[10] but, despite studies of cascades in a waste glass[11] and in zircon,[12] less attention has been paid to the mechanism of damage production in displacement cascades in ceramics. The structure and the initial evolution of the radiation-damaged state are increasingly accessible to study with current computational resources. Here, we investigate and compare the formation of cascades in $Gd_2Ti_2O_7$ and $Gd_2Zr_2O_7$.

Methodology

Molecular dynamics simulations are well suited to studying atomic processes that operate on picosecond time scales and we have employed the DLPOLY code[13] for this purpose. The ionic model was used exclusively throughout. Each ion was assigned its formal charge, *i.e.* 3+, 4+ and 2− for Gd, Ti/Zr and O, respectively. During a displacement cascade, ions can approach each other very closely and, for the non-Coulombic

Table 1 Short-range potential parameters. The form of the Buckingham potential is $V_{ij} = A\exp(-r_{ij}/\rho) - C/r_{ij}^6$

Interaction	A/eV	ρ/Å	C/eV Å^6
O–O	249.3764	0.3621	0.0
Ti–O	3874.4	0.2717	0.0
Gd–O	4651.9633	0.2923	0.0
Zr–O	8769.5930	0.2619	4.581

interactions, it is important to use potentials that are likely to be accurate over a wide range of internuclear separations. We avoided potential sets that include a large attractive Cr^{-6} term (where C is a constant and large in this context signifies $C > \approx 20$ eV Å^6), since this creates an unphysical infinite well at small interionic separations and may lead to implosion of the simulation. The potentials used here have been calculated over a wide range of separations using a modified Gordon–Kim approach.[14] The parameters listed in Table 1 were obtained by fitting an exponential of the form $A\exp(-r/\rho)$ (where A and ρ are constants) to the electron–gas interaction energies of ref. 15. In one case (Zr^{4+}–O^{2-}), a Cr^{-6} term was required in the fitting and a small value of C obtained; results for undefective $Gd_2Zr_2O_7$, omitting this term, differ only slightly from those reported below.

These electron–gas potentials have been used previously in simulation studies of a wide range of binary and ternary oxides (*e.g.* high temperature superconducting ceramics[15]), and have been particularly useful for problems involving defects where the interatomic distances close to the defect after relaxation may be very different from in the perfect lattice at equilibrium.[14,16] Lattice parameters and selected bond lengths for undefective $Gd_2Ti_2O_7$ and $Gd_2Zr_2O_7$, calculated using energy minimisation in the static limit using the GULP code,[17] are compared with the experimental values[8,18,19] in Table 2. It is worth noting the work of Minervini *et al.*,[20] who concluded that in pyrochlores, the oxygen atom position (48f) and, hence, the bond lengths are sensitive to the intrinsic disorder, which is ignored in these minimisations.

Results and discussion

The production of a cascade was started from the energetic recoil of a single atom, the PKA, and the subsequent collisions, displacements and recombination of atoms with vacant sites followed, so that the complete structure and evolution of the cascade could be monitored. The size of the block of atoms was chosen so that the cascade did not overlap significantly with its periodic image. For PKAs with energies $E < 1$ keV and 1 keV$< E <$ 20 keV, cubic simulation cells containing 88 000 and 193 336 atoms were used, respectively. Initial simulation cell lengths were set to the appropriate multiple of the experimental lattice parameter, corresponding to 10 and 13 unit cells in each direction, respectively. The initial temperature of the simulation was set to 300 K and the simulation allowed to equilibrate for 10 ps (3 ps for the largest cell) within the NPT ensemble. A PKA was then chosen at random and set moving in a random direction and the simulation allowed to proceed using the Verlet algorithm within the NVE ensemble for a further 5 ps (2.5 ps for the largest cell). The timestep for all simulations was 0.5 fs. The creation of a radiation cascade results in an initial spike in the global temperature of the simulation cell, no larger than 400 K (due to the large size of the simulation cell), and the temperature then decreases during the simulation.

A key parameter to determine the resistance of a structure to radiation damage is the number of defects created as a function of the PKA energy. The behaviour of metals, in which cascades can be analysed in terms of point-defect assemblies, is quite different. For metals, a distinction is made between replacement, where an atom takes the place of an equivalent atom in the crystalline structure, and displacement, where an atom at the end of the cascade occupies an interstitial position. It is impossible to analyse the tracks in $Gd_2Ti_2O_7$ in this way, since they are amorphous and the occupancy of crystal sites in the track after the cascade cannot be defined. We define, following ref. 10, a defect as an ion that has moved more than the average of the first neighbour interatomic distances. This is determined with respect to the position of an ion after the equilibration phase of the simulation, and includes ions that have been both displaced and replaced.

The duration of this subsequent simulation of the cascade evolution might influence the number of calculated defects if the simulation is truncated prematurely, and so the number of defects was monitored as a function of time. Fig. 1(a) shows the results of a single simulation, using a PKA of 20 keV (the highest energy considered in this study), and it is evident that after approximately 2.5 ps, the number of defects remains

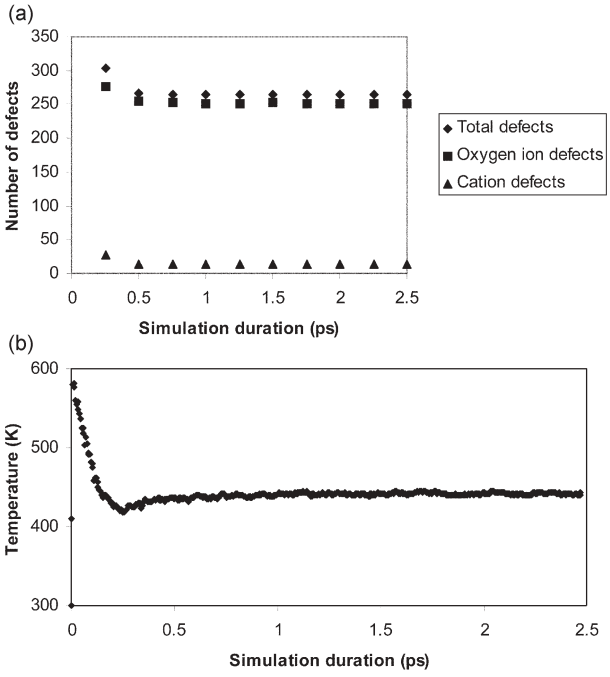

Fig. 1 Number of defects (a) and temperature (b) as a function of time after the creation of a PKA for a single simulation on $Gd_2Zr_2O_7$. The 20 keV PKA was a Gd ion in this case. As discussed in the text, we define a defect as an ion that has moved more than the average of the first neighbour interatomic distances.

Table 2 Calculated (static limit) and experimental lattice parameters and bond lengths for $Gd_2Zr_2O_7$ and $Gd_2Ti_2O_7$

	$Gd_2Zr_2O_7$ (calc.)	$Gd_2Zr_2O_7$ (expt.)[18]	$Gd_2Ti_2O_7$ (calc.)	$Gd_2Ti_2O_7$ (expt.)[19,a]
Lattice parameter/Å	10.758	10.523	10.191	10.185
Average bond lengths/Å				
Gd–Zr	3.804	3.720	3.603	3.601
Gd–O	2.557	2.445	2.471	2.459
Zr/Ti–O	2.091	2.093	1.943	1.951

[a]In addition, ref. 8 reports a lattice parameter of 10.193 Å for $Gd_2Ti_2O_7$ from X-ray diffraction.

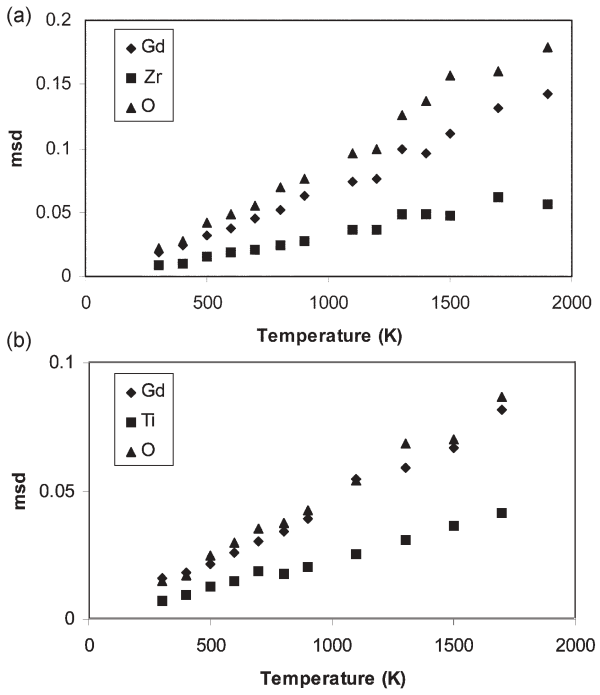

Fig. 2 Mean-square displacements ($Å^2$) for (a) $Gd_2Zr_2O_7$ and (b) $Gd_2Ti_2O_7$ as a function of temperature.

constant. Temperature is shown as a function of time for this simulation in Fig. 1(b). To investigate whether defect diffusion takes place after the number of defects is effectively constant, we have carried out a series of NPT simulations on $Gd_2Zr_2O_7$ and $Gd_2Ti_2O_7$ (20 ps duration) and determined the limiting value of the mean-square displacement over a range of temperatures considerably wider than the variation of the global temperature of the cell [Fig. 1(b)]. The results, shown in Fig. 2, indicate self-diffusion processes are negligible after the final formation of the cascade and will not influence the number of defects on this relatively short timescale.

Since each cascade is different, it is necessary to simulate as many cascades as possible in order to collect reasonable statistics and identify trends. Unfortunately, limitations in computer resources hinder this objective (especially for the largest cell). Five simulations were performed for cascades with PKA energy < 10 keV and two for the largest energies (*i.e.* those containing 193 336 ions). The largest simulations took several weeks of CPU time on four 833 MHz EV68 processors on the Mott Compaq supercomputer cluster at RAL.

Fig. 3 displays the number of defects as a function of energy

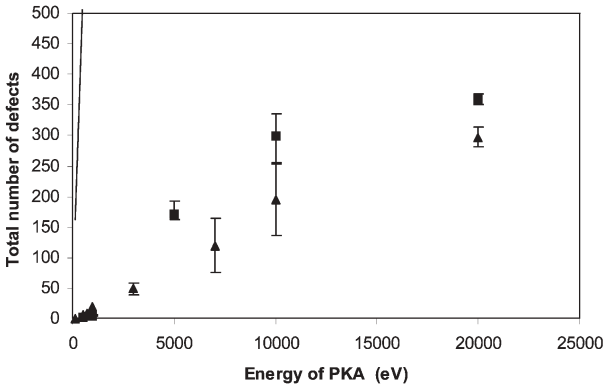

Fig. 3 Total mean number of defects created as a function of PKA energy for $Gd_2Zr_2O_7$ (triangles) and $Gd_2Ti_2O_7$ (squares). The definition of a defect is as in Fig. 1. For comparison, the solid line on the left-hand side is for Cu (taken from ref. 10). The 'error bars' represent the maximum and minimum number of defects for a given PKA energy.

of the PKA. For comparison, the solid line on the left-hand side of this figure is for Cu (from ref. 10). We were unable to determine, within the uncertainty in the simulations, whether the mass of the PKA significantly affected the number of defects created. A similar situation has been observed in simulations of Cu–Au solid solutions.[10] Clearly, the number of defects created is much larger in $Gd_2Ti_2O_7$ than in $Gd_2Zr_2O_7$, which supports the results of the high energy ion bombardment experiments of ref. 4, in which resistance to amorphisation increased markedly with increasing Zr content. It is of course possible to use an alternative definition of a 'defect' with a different deviation distance. In the course of the analysis, we examined several such distances from 1 Å upwards. As anticipated, the number of defects varies with this cutoff, but all the differences we note between $Gd_2Ti_2O_7$ and $Gd_2Zr_2O_7$ remain unchanged.

The typical structures of a displacement cascade in $Gd_2Zr_2O_7$ and in $Gd_2Ti_2O_7$ are displayed in Fig. 4 and 5, respectively. The cascade structure of $Gd_2Zr_2O_7$ tends to be elongated (roughly cylindrical) and the displaced ions form an 'ordered' structure. In this context, it is instructive to consider the ionic conductivity measurements for the ZrO_2–Gd_2O_3 system.[21] The pyrochlore $Gd_2Zr_2O_7$ shows enhanced

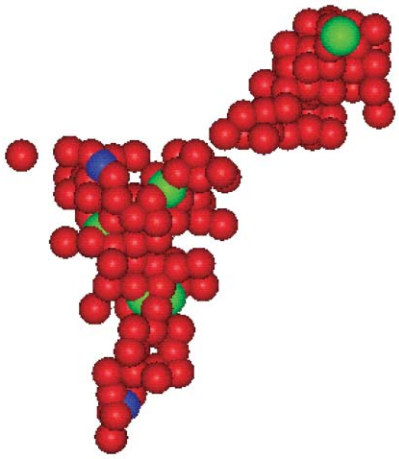

Fig. 4 Typical structure of a defect cascade in $Gd_2Zr_2O_7$. This example is for a PKA of 10 keV. Oxygen ions are red, Gd green and Zr blue.

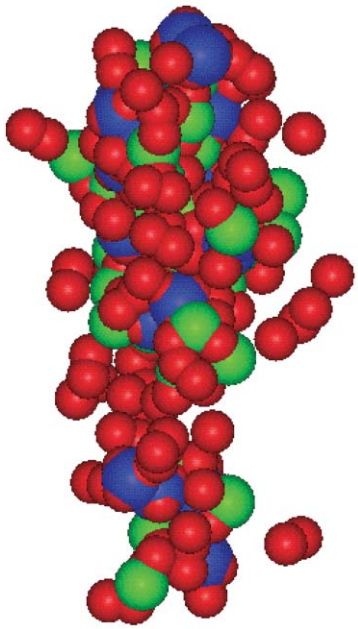

Fig. 5 Typical structure of a defect cascade in $Gd_2Ti_2O_7$. This example is for a PKA of 10 keV. Oxygen ions are red, Gd green and Ti blue.

conductivity relative to the defect fluorite phases, which bound it at either side in the phase diagram. The pyrochlore structure not only contains A and B ions on separate sublattices, but the seven oxygen ions per formula unit in the unit cell also fully occupy two sublattices (48f and 8b). Unlike the defective fluorite structure, there is an ordered arrangement of oxygen vacancies, with the so-called 8a site vacant. The ionic conductivity is due to intrinsic disorder of oxygen ions between the occupied 48f and empty 8a sites.[15] Within the cascade, the oxygen ions also tend to be associated with this 8a site (*i.e.* within 0.5 Å of the 8a position).

In contrast, $Gd_2Ti_2O_7$ cascades tend to be more ellipsoidal in shape and are amorphous. Similar structures have been observed in simulations of zircon.[12] We note that for $Gd_2Ti_2O_7$, intrinsic oxygen disorder, and hence ionic conductivity, is negligible.[22] Our calculations also indicate that the ratio of oxide to cation defects is different for the two compounds. In $Gd_2Ti_2O_7$ the ratio of defects is roughly in proportion to the stoichiometry (within a unit cell of 88 ions there are 24 cations, *i.e.* $\approx$27%). In contrast, only approximately 10% of defects in $Gd_2Zr_2O_7$ are cations. This tends to be more pronounced at lower PKA energies, which indicates that the activation energy for displacement of the oxygen ions is less than that for the cations.

Of the two materials $Gd_2Zr_2O_7$ appears more resistant to the creation of interstitial ions and vacancies than $Gd_2Ti_2O_7$. Global amorphisation processes have been classified as follows:[12,23,24] (1) amorphisation during a single impact (within a cascade); (2) overlap of cascades, each of which has produced an array of point defects, thereby creating an amorphous area in the crystal; (3) a composite model in which a cascade produces a central amorphous zone and a number of peripheral damaged zones subject to further amorphisation from the overlap of subsequent cascades.

Our calculations suggest that either the direct impact and/or composite model is appropriate for $Gd_2Ti_2O_7$, whereas the overlapping cascade model is applicable to $Gd_2Zr_2O_7$. A single cascade in $Gd_2Zr_2O_7$ tends to produce an ordered array of point defects. This ability to undergo an order–disorder transition may provide $Gd_2Zr_2O_7$ with greater propensity to resist radiation damage.[5]

At this point, it is worth mentioning the comprehensive studies of Grimes and co-workers[5,20,25] on point-defect energies in pyrochlores. Their calculated point-defect energies (in the dilute limit) associated with (i) a cation-antisite defect and (ii) a cation-antisite defect adjacent to an anion Frenkel pair are as much as several eV lower in energy for $Gd_2Zr_2O_7$ than for $Gd_2Ti_2O_7$. We have also calculated these defect energies for the two materials using the two-region Mott–Littleton approach[26] and the GULP code.[17] Our values are close to those in ref. 5 and 25, with a difference of $\sim$3 eV in the energies of these defects between the two compounds. There appears to be a useful correlation (structure–activity relationship) between these point-defect energies and the extent of radiation damage; compounds with high defect energies seem to be more suspectible to amorphisation.

Our simulations have been limited to small initial PKA energies because of the problem of cascade overlap. While molecular dynamics simulations include crystal structure effects and a realistic treatment of atomic movements during the cascade, we are restricted by the size of the simulation cell. In addition, as pointed out in ref. 6, the creation of a defect cascade is only part of the process of the formation of the damaged state. Our simulations, due to the short timescale, are not able to probe the healing process and determine the ultimate fate of the interstitial ions and vacancies (*i.e.* the formation of defect clusters and dislocations) and further work of this nature is required. However, we expect thermal annealing *via* order–disorder in $Gd_2Zr_2O_7$ (which is an ionic conductor) to be faster than for structural recovery from an amorphous state as in $Gd_2Ti_2O_7$.

Acknowledgements

This work was supported by EPSRC grant GR/M34799 and time on the Mott 20-processor Compaq supercomputer cluster at RAL was purchased and supported *via* a HEFCE/Compaq JREI award (JR99BAPAEQ).

References

1 K. K. S. Pillay, *Radwaste*, 1996, Jan, 60.
2 G. Taubes, *Science*, 1994, **263**, 629.
3 S. X. Wang, L. M. Wang, R. C. Ewing and K. V. Govindan Kutty, *Nucl. Instrum. Methods Phys. Res., Sect. B*, 2000, **169**, 135.
4 S. X. Wang, B. D. Begg, L. M. Wang, R. C. Ewing, W. J. Weber and K. V. Govindan Kutty, *J. Mater. Res.*, 1999, **14**, 4470.
5 K. E. Sickafus, L. Minervini, R. W. Grimes, J. A. Valdez, M. Ishimaru, F. Li, K. J. McClellan and T. Hartmann, *Science*, 2000, **289**, 748.
6 W. J. Weber and R. C. Ewing, *Science*, 2000, **289**, 2051.
7 H. C. Gupta, S. Brown, N. Rani and V. B. Gohel, *J. Raman Spectrosc.*, 2001, **32**, 41.
8 N. J. Hess, B. D. Begg, S. D. Conradson, D. E. McCready, P. L. Gassman and W. J. Weber, *J. Phys. B*, 2002, **106**, 4663.
9 W. J. Weber, R. C. Ewing, C. R. A. Catlow, T. Diaz de la Rubia, L. W. Hobbs, C. Kinoshita, Hj. Matzke, A. T. Motta, M. Nastasi, E. K. H. Salje, E. R. Vance and S. J. Zinkle, *J. Mater. Res.*, 1998, **13**, 1434.
10 H. F. Deng and D. J. Bacon, *Phys. Rev. B*, 1996, **53**, 11376.
11 J. M. Delaye and D. Ghaleb, *J. Nucl. Mater.*, 1997, **244**, 22.
12 J.-P. Crocombette and D. Ghaleb, *J. Nucl. Mater.*, 2001, **295**, 167.
13 T. R. Forester and W. Smith, DLPOLY, CCLRC, Daresbury Laboratory, Warrington, UK, 1995.
14 N. L. Allan and W. C. Mackrodt, *Philos. Mag. B*, 1994, **69**, 871.
15 N. L. Allan and W. C. Mackrodt, *Adv. Solid State Chem.*, 1993, **3**, 221.
16 N. L. Allan and W. C. Mackrodt, *Mol. Simul.*, 1994, **12**, 89.
17 J. D. Gale, *J. Chem. Soc., Faraday Trans.*, 1997, **93**, 629.
18 T. Moriga, A. Yoshiasa, F. Kanamaru, K. Koto, M. Yoshimura and S. Somiya, *Solid State Ionics*, 1989, **31**, 319.
19 O. Knop, F. Brisse and L. Castelliz, *Can. J. Chem.*, 1969, **47**, 971.
20 L. Minervini, R. W. Grimes, Y. Tabira, R. L. Withers and K. E. Sickafus, *Philos. Mag. A*, 2002, **82**, 123.
21 M. P. van Dijk, K. J. de Vries and A. J. Burggraaf, *Solid State Ionics*, 1983, **9/10**, 913.
22 H. L. Tuller, *J. Phys. Chem. Solids*, 1994, **55**, 1393.
23 R. Webb and G. Carter, *Radiat. Eff.*, 1979, **42**, 159.
24 W. J. Weber, *J. Mater. Res.*, 1995, **5**, 2687.
25 L. Minervini, R. W. Grimes and K. E. Sickafus, *J. Am. Ceram. Soc.*, 2000, **83**, 1873.
26 A. B. Lidiard, *J. Chem. Soc., Faraday Trans. 2*, 1989, **85**, 341.